

# Nonequilibrium Roughness Evolution of Small Molecule Mixed Films Reflecting Equilibrium Phase Behavior

Alexander Hinderhofer,\* Jan Hagenlocher, Alexander Gerlach, Joachim Krug, Martin Oettel, and Frank Schreiber



Cite This: *J. Phys. Chem. C* 2022, 126, 11348–11357



Read Online

ACCESS |



Metrics & More

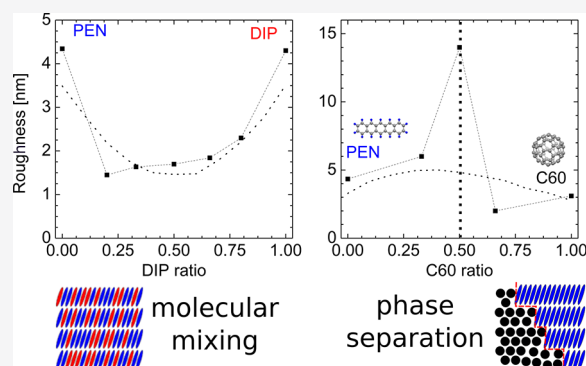


Article Recommendations



Supporting Information

**ABSTRACT:** Understanding nonequilibrium phenomena, such as growth, and connecting them to equilibrium phase behavior is a major challenge, in particular for complex multicomponent materials. We use X-ray reflectivity to determine the surface roughness of binary mixtures of several prototypical organic compounds. By analyzing the roughness as a function of composition, we find a systematic behavior depending on the bulk phase behavior in terms of intermixing, co-crystallization, or phase separation. Supported by kinetic Monte Carlo simulations, we provide evidence that the growth behavior can be rationalized by a lowered step edge barrier in the mixed films which is induced by reduced in-plane crystallinity.



## INTRODUCTION

Structure formation involves intriguing aspects of non-equilibrium statistical physics. Complexity arises from the fact that, in contrast to equilibrium thermodynamics, it is not sufficient to determine only the lowest free energy state, although the equilibrium scenario is expected as a limiting case. A typical example for a nonequilibrium system is thin film growth, where a large variety of morphologies can be observed, which cannot be explained solely by equilibrium considerations. Instead, kinetic effects play a strong role in the formation of microscopic and mesoscopic structures. A key observable to characterize the growth behavior is the surface roughness ( $\sigma$ , standard deviation of the film thickness), which is also of substantial technological importance.<sup>1–5</sup>

The growth of molecular thin films was studied extensively both theoretically<sup>6–8</sup> and experimentally.<sup>9–14</sup> Frequently, a typical feature for crystalline molecular films is the comparably fast roughening, often expressed as a high roughening exponent.<sup>12,15,16</sup> The complex roughening behavior is explained predominantly by kinetic effects based on high step edge barriers,<sup>17–21</sup> thickness-dependent strain release,<sup>15</sup> or a restricted diffusion length due to defects or grain boundaries.<sup>22</sup>

More challenging cases for complex materials are binary molecular systems, which are also important due to their electronic properties. Molecular mixed thin films are studied both with small mixing ratios ( $\approx 1:100$ )<sup>23–25</sup> for doping as well as large mixing ratios ( $\approx 1:1$ ) for bulk heterojunctions and molecular complex formation.<sup>26–34</sup> Dependent on the effective interactions of the compounds, binary systems exhibit several different mixing behaviors in the bulk, such as solid solution,

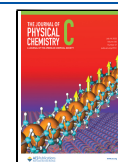
co-crystallization, or phase separation.<sup>27,35</sup> The structure and morphology resulting from the growth, including the distribution of the two components A and B, strongly impact the effective electronic and optical properties and thus ultimately device performance. From the growth perspective, the relationship between mixing behavior in equilibrium and kinetically determined surface roughness is of significant fundamental interest.

Here, we demonstrate that the mixing ratio and bulk phase behavior correlate strongly with kinetically limited growth effects and specifically with the roughness evolution. We provide a comprehensive study of a broad range of blends with different electronic and steric characteristics. Supported by kinetic Monte Carlo (KMC) simulations, we identify three main effects: (1) A general smoothing effect for mixed films is induced by a lowered step edge barrier compared to the pure films. (2) Mixtures forming a co-crystal exhibit a local roughness maximum at a 1:1 mixing ratio, because pure phase systems exhibit an increased step edge barrier compared to random mixtures. (3) Strongly phase separating mixtures exhibit increased roughness due to 3D island growth on a larger lateral scale.

Received: March 30, 2022

Revised: June 3, 2022

Published: July 5, 2022



The experiments are performed with a rich variety of molecular species, differing in shape and interaction anisotropy. In order to identify the generic behavior, in our simulation approach, we model the two-component systems generically with a simple binary lattice gas (species A and B). The static parameters governing the equilibrium phase behavior are given by nearest-neighbor interaction energies  $\epsilon_{ij}$  ( $i, j = \{A, B\}$ ) and substrate interaction energies  $\epsilon_{\text{sub}}^A$  and  $\epsilon_{\text{sub}}^B$  for particles in the first layer (see Figure 1). Film growth is

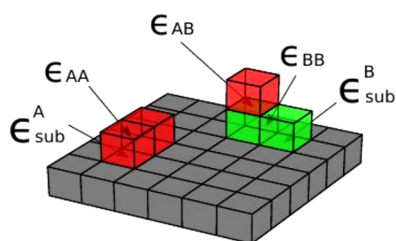


Figure 1. Energy parameters in the binary lattice gas model.

modeled with KMC simulations with solid-on-solid restrictions, and the associated dynamic parameters are (i) free diffusion constants  $D_{A[B]}$  for a particle of species A[B] which is not laterally bound, (ii) a deposition rate  $F$  (particles per unit of time and lattice site), and (iii) species-dependent Ehrlich–Schwoebel barriers  $E_{ij}^{\text{ES}}$ . (An important dimensionless ratio determining the degree of nonequilibrium is given by  $\Gamma = D_A/F$ .) All energetic parameters are given in units of the thermal energy.

We stress that we use the simple solid-on-solid model mainly as a conceptual tool. The model is clearly not material-specific, nor is it intended to faithfully represent the microscopic molecular moves and their associated rates. We also work with lower interaction energies and higher deposition rates than in the experiment. However, the simplicity of the model allows one to uncover and quantify the three generic effects described above and to exclude other possible sources of the observed roughness behavior. As detailed molecular simulations of binary growth systems with realistic parameters are currently out of reach, this strategy appears to be most appropriate for elucidating the universal patterns that we see. Currently, specific growth effects in one-component systems can be investigated using molecular dynamics simulations as recent examples for C60 growth<sup>36</sup> or pentacene growth<sup>18,37,38</sup> show. Generic effects, however, could only be addressed by extending simulations to mixtures and treating a wide range of molecular species and compositions, which appears to be unrealistic.

In the following, we will first discuss the roughness evolution of binary mixtures of rodlike compounds which are not phase-separating but may show the formation of co-crystals. In the second part, we will discuss the phase separating rod/sphere-shaped mixed films.

## METHODS

**Thin Film Preparation.** All films studied have a thickness of nominal 20 nm and were prepared by thermal evaporation in vacuum onto Si wafers with native oxide layer. Thin films were deposited on silicon wafers with native SiO<sub>2</sub> (surface roughness  $\sigma_{\text{rms}} = 0.3$  nm) under ultrahigh vacuum (UHV) conditions (base pressure  $< 1 \times 10^{-7}$  Pa) by thermal evaporation.<sup>39</sup> Before deposition, substrates were cleaned ultrasonically with acetone, isopropyl alcohol, and ultrapure

water, followed by heating to 700 K in the UHV growth chamber. All films were deposited at a substrate temperature of  $T \sim 300$  K. The growth rate was monitored by using a quartz crystal microbalance. Typical evaporation rates are shown in Table S1. The estimated error of the stoichiometry of the mixtures is about 10% determined by the error of the quartz crystal microbalance.

Pentacene (PEN) was purchased from Sigma-Aldrich, (99.9% purity), diindenoperylene (DIP) was from Institut fuer PAH Forschung Greifenberg, Germany, (99.9% purity), picene (PIC) was from NARD Co. (99.9% purity), perfluoropentacene (PFP) was from (Kanto Denka Kogyo Co. (99% purity), *N,N'*-bis(2-ethyl-hexyl)-1,7-dicyanoperylene-3,4/9,10-bis(dicarboxyimide) (PDIR-CN<sub>2</sub>) was from Polyera, U.S.A. (99% purity), fullerene (C60) was from Creaphys (99.9% purity), and sexithiophene (6T) was from Sigma-Aldrich (80% initial purity and purified twice by temperature gradient sublimation before film preparation).

**X-ray Scattering.** X-ray reflectivity (XRR) and grazing incidence X-ray diffraction (GIXD) were measured either at the X04SA beamline of the Swiss Light Source, Paul Scherrer Institut, Villigen, Switzerland or at beamline ID10 of the ESRF in Grenoble, France. Films were measured at different beam times with beam energies between 9.7–20 keV. Typical beam sizes determined by detector slits were 0.03 mm in vertical direction and 0.1 mm in horizontal direction. GIXD measurements were done close to the critical angle for each sample to increase the scattering amplitude. All measurements were performed either under vacuum or under He atmosphere to reduce air scattering. Some additional XRR data were obtained with a GE-Seifert X-ray reflectometer using Cu  $K_{\alpha 1}$  radiation (8.05 keV).

**Atomic Force Microscopy.** The morphology was investigated by atomic force microscopy (AFM) using a JPK NanoWizard II instrument in tapping mode under ambient conditions. The resonant frequency of the cantilever used was about 300 kHz. The pyramidal-shaped tip was made of silicon and had a tip radius of less than 10 nm. The images were collected at a scan rate of 0.5 lines per second.

**Roughness Determination.** Roughness ( $\sigma$ ) values were determined by fitting XRR with Motofit<sup>40</sup> and from AFM with Gwyddion.<sup>41</sup> Both methods yielded very similar results. We estimate the error bars for the  $\sigma$  values on the range of 10%.

**In-Plane Coherent Crystal Size.** Lower limits of the in-plane coherent crystal sizes  $d_{\text{coh}}$  were determined by the Scherrer formula  $l_s = 2\pi \times (\text{fwhm})^{-1}$ , where fwhm is the full width half-maximum of the peak in  $\text{\AA}^{-1}$  determined with a Gaussian fit-function.<sup>42</sup> The instrumental broadening of the diffractometer was not included in the calculation; therefore, only lower limits of  $l_s$  are given.

**In-Plane Correlation Length.** In-plane correlation lengths were determined with Gwyddion<sup>41</sup> from AFM data by fitting the one-dimensional power spectral density function (PSDF) with a power law. The used PSDF for each sample is an average from two to four images with sizes between 3 and 10  $\mu\text{m}$ .

**Simulation Model.** For the KMC simulations, we employ a simple film growth model using a binary lattice gas (species A and B) on a cubic lattice with interaction energy parameters as illustrated in Figure 1. Deposition on top of the film or the bare substrate at random substrate plane coordinates is controlled by a rate  $F$  (particles per unit time and lattice site). Diffusion respects the solid-on-solid condition: only the

particles (species  $i$ ) in the top layer are allowed to diffuse to a lateral next-neighbor site with rate  $D_i \min(1, \exp(-\Delta E))$ , where  $D_i$  is a species-dependent free diffusion constant and  $\Delta E$  is the energy difference between final and initial state in units of  $k_B T$ . In such a move, particles of species  $i$  may also ascend (moving on top of a particle of species  $j$ ) or descend one layer (moving down from a particle of species  $j$ ), in which case the rate is multiplied with  $\exp(-E_{ij}^{ES})$ , where  $E_{ij}^{ES}$  is an Ehrlich–Schwoebel (ES) barrier. Neither overhang nor desorption is allowed. The moves are illustrated in Figure 2.

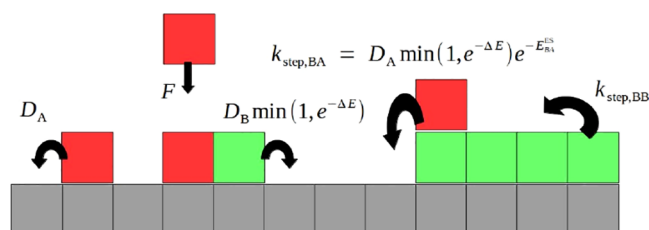


**Figure 2.** Hopping and insertion moves with associated rates in the KMC model.

In the one-component case (Figure S3), the model is characterized by the four constants  $\epsilon = \epsilon_{AA}$ ,  $\epsilon_{\text{sub}} = \epsilon_{\text{sub}}^A$ ,  $E^{ES} = E_{AA}^{ES}$ , and  $\Gamma = D_A/F$ . Actual growth experiments of organic thin films are characterized by  $|\epsilon| = 10\text{--}15$  and  $\Gamma = 10^9\text{--}10^{11}$  which is difficult to simulate, due to computational costs. However, at lower energies and smaller ratios  $\Gamma$ , the model shows similar growth modes as seen experimentally. These are (a) island growth from the start (ISL) when  $\epsilon_{\text{sub}}$  is low enough, (b) layer-by-layer growth (LBL), and (c) 3D growth of varying degree. The model shows two characteristic transitions which, however, are not sharp: (i) ISL-LBL which for a given  $\epsilon$  and  $E^{ES}$  depends on both  $\epsilon_{\text{sub}}$  and  $\Gamma$  and whose order parameter can be characterized by the coverage difference of layer 1 and 2 after depositing only 1 ML. (ii) LBL-3D, respectively, ISL-3D which for a given  $\epsilon$ ,  $\epsilon_{\text{sub}}$ , and  $E^{ES}$  depends on  $\Gamma$  and where a suitable order parameter is, e.g., the integral of the anti-Bragg intensity and needs deposition of tens of MLs for locating.

More details on the one-component growth modes and the associated transitions can be found in ref 43.

**Simulation Parameter Selection.** In selecting the parameters for the pure systems, we proceed with the assumption that there are scaling relations for the temporal roughness evolution, i.e., that simulations at lower  $|\epsilon|$ ,  $\epsilon_{\text{sub}}$ ,  $E^{ES}$ , and  $\Gamma$  correspond also to certain sets of these parameters with higher values. In the literature, the epitaxial case  $\epsilon = \epsilon_{\text{sub}}$  and  $E^{ES} = 0$  has been investigated recently<sup>44</sup> and a scaling  $r \propto L^\beta / (\Gamma^{3/2} (\exp(-|\epsilon|) + a))$  has been found ( $r$  is the normalized roughness with a layer thickness of 1,  $L$  is the number of deposited layers,  $\beta \approx 0.2$ ,  $a = 0.025$ ).

We have investigated the scaling relations for the exemplary case of the PEN:DIP mixtures for energy parameters  $\epsilon = -3$  to  $-5$  and a wider range of diffusion parameters  $\Gamma = D_A = D_B = 10^3\text{--}10^6$ . We found that the composition dependence of a multilayer film depends rather well on the single variable  $\Gamma^{1.5} \exp(-|\epsilon|)$  which was also found in the single-component case by Assis and Aarão Reis.<sup>44</sup> Thus, e.g., when coming from a more realistic energy scale of  $\epsilon = -15$  to  $\epsilon = -3$ , one may reduce  $\Gamma$  by a factor of  $2 \times 10^3$  if that scaling holds.

In going to growth of binary systems, the dimension of the parameter space of this simple model is already enlarged to 10

(4 parameters for each of the pure systems, the cross-species energy  $\epsilon_{AB}$  (which controls mixing and demixing) and the cross-Ehrlich–Schwoebel barrier  $E_{AB}^{ES} = E_{BA}^{ES}$ ). We concentrated on combining different pairs of one-component growth modes which reflect the experimental material combinations. In general, we found that for the simple choices  $\epsilon_{AB} \approx (\epsilon_{AA} + \epsilon_{BB})/2$ ,  $D_A \approx D_B$ , and  $E_{ij}^{ES} = \text{const}$  the roughness properties of the films linearly interpolate between those of the pure substances. Therefore, any more prominent mixture effects can only be expected when deviating from these choices.

Simulations were done on a square grid with lateral size of  $M = 300$ . Our tests for larger grid sizes ( $M = 800$ ) show that the obtained roughness values do not depend strongly on the grid size (Figure S5).

## RESULTS AND DISCUSSION

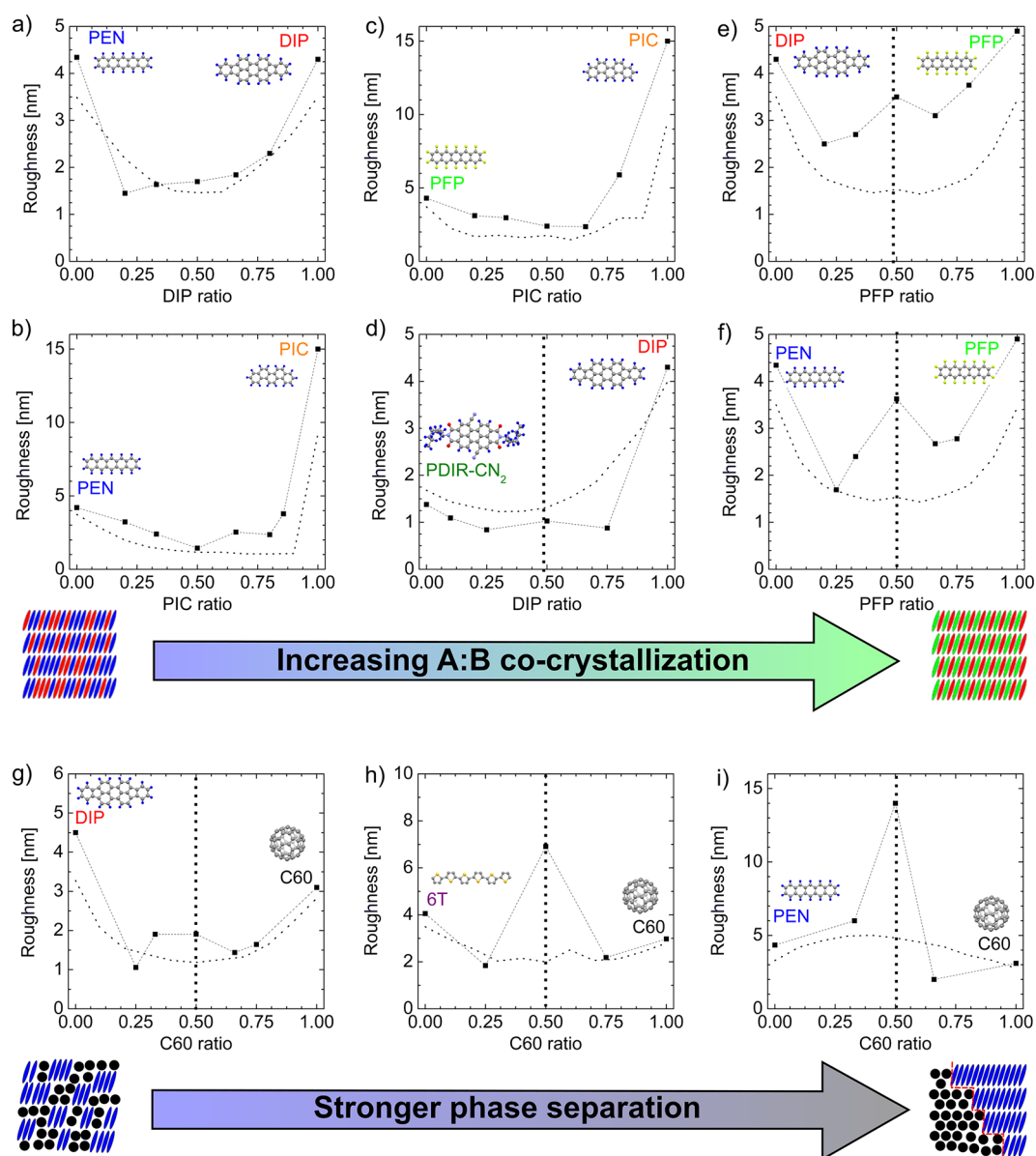
**Roughness of Intermixing Thin Films.** In pure thin films, most of the studied compounds, i.e. pentacene (PEN), perfluoropentacene (PFP), diindenoperylene (DIP), sexithiophene (6T), and  $N,N'$ -bis(2-ethyl-hexyl)-1,7-dicyanoperylene-3,4/9,10-bis(dicarboxyimide) (PDIR-CN<sub>2</sub>, where  $R = C_8H_{17}$ , branched)<sup>31</sup> exhibit so-called layer-plus-island growth (Stranski–Krahanov, SK) on SiO<sub>2</sub> under the conditions employed here. In addition, picene (PIC) and fullerene (C60) exhibit typically island growth without a wetting layer (Volmer–Weber, VW). The growth conditions of the single component films and the studied mixed films are summarized in Table S2.

Figure 3a–f shows the roughness of six different types of molecular mixed films dependent on mixing ratio at a thickness of 20 nm. All of the studied binary compounds mix on the molecular level, but they can be distinguished by their tendency to form a co-crystal.<sup>28–34</sup> The roughness of all pure materials is in general relatively large. A systematic trend in all films is that, upon mixing, the roughness is strongly decreased.

By comparing the roughness dependence of the various mixed systems, we can observe some significant differences. Mixtures with strong co-crystallization, i.e., the formation of an equimolar ordered co-crystal, exhibit a local roughness maximum at a 1:1 ratio (Figure 3e,f). In contrast, solid solutions do not show this local maximum (Figure 3a,b), which will be discussed in detail further below.

We find for mixtures with PIC the strongest smoothing effect in absolute terms (Figure 3b,c). Pure PIC exhibits strong island growth (VW) on SiO<sub>2</sub> substrates.<sup>45–47</sup> Upon mixing, the growth mode is apparently changed to SK mode. This effect is observable for PEN:PIC and PFP:PIC blends even for very low PEN or PFP concentrations. The smoothing in mixtures is observed not only for mixtures with a compound showing strong islanding (SK:VW) but also for mixtures where both compounds exhibit SK growth mode such as PEN, PFP and DIP. In order to better understand the overall picture, we discuss possible smoothing mechanisms and compare them to experimental results and theoretical simulations.

**Nucleation Density.** As a possible smoothing mechanism, we consider first an increased nucleation density in the mixtures, which would yield a lower roughness via a simple geometric argument (Figure S1).<sup>48</sup> The increase in nucleation density would in turn lead to a reduced in-plane correlation length  $\xi$ . However, judging from the in-plane correlation length extracted from AFM data (Figure S1), we cannot identify a clear dependence between in-plane correlation



**Figure 3.** Roughness  $\sigma$  of mixed films (20 nm thickness) with rodlike compounds (a–f) dependent on mixing ratio: (a) PEN:DIP,<sup>28</sup> (b) PEN:PIC,<sup>29,30</sup> (c) PFP:PIC,<sup>29</sup> (d) DIP:PDIR-CN<sub>2</sub>,<sup>31</sup> (e) DIP:PFP,<sup>32,33</sup> and (f) PEN:PFP.<sup>34</sup> From (a) to (f), the in-plane co-crystallization is increasing, i.e., PEN:DIP mixtures are nearly randomly intermixing, whereas PEN:PFP mixtures exhibit well ordered co-crystallization and (b)–(e) are intermediate cases. (g–i) Roughness  $\sigma$  of phase separating compounds: (g) DIP:C60, (h) 6T:C60, and (i) PEN:C60. The degree of phase separation is increasing from (g) to (i). Local roughness maxima at ratio 0.5 are marked by vertical lines. All  $\sigma$  values were determined by XRR, except those for pure PIC and mixtures of PEN:C60 and 6T:C60, which were determined by AFM. Simulated roughness values are shown as dotted lines. Simulation parameters are listed in Table S3.

length and roughness. Therefore, we rule out this smoothing mechanism as being generally operational.

**Molecular Orientation.** Due to their anisotropic nature, a change in molecular orientation may change the roughening behavior of single component films drastically. For example, PEN deposited on differently modified Au surfaces exhibit a change in orientation and consecutively the growth mode.<sup>49</sup> For the material combinations studied here, all rod-like molecules have a nearly upright standing orientation in single component films on Si wafers with native oxide layer. Based on GIXD data of previous studies,<sup>28–34</sup> we do not observe strong orientational changes even upon mixing except for both PEN:PFP and DIP:PFP. There, the 1:1 co-crystal phase might undergo a thickness dependent orientation change from nearly

upright standing molecules to nearly lying molecules.<sup>32,34,50</sup>

This orientation change is more pronounced for mixing ratios near 1:1 and might play a small additional role for the increased roughness at these mixing ratios in co-crystals. However, apart from this observation for the co-crystalline systems, which are discussed further below, we do not observe any hints of orientational changes and therefore exclude these as strong contributors to the observed roughening.

**Interaction Strength and Diffusion Rate.** Two additional possible smoothing mechanisms may be that an increase in diffusion rate or a different interspecies interaction strength in the blend affects the roughness. On the one hand, a higher diffusion rate in the mixed film compared to the pure film would increase the hopping rate over step edges and lead

potentially to smoother films. On the other hand, an increased interspecies interaction in the mixed films may reduce the roughness, because smoother films are energetically favored.

Experimentally, it is difficult to vary these two types of parameters systematically and independently. This can be done in our generic model. To test the impact of interspecies interaction strength, we set  $D = D_A = D_B$  (Figure 4). We

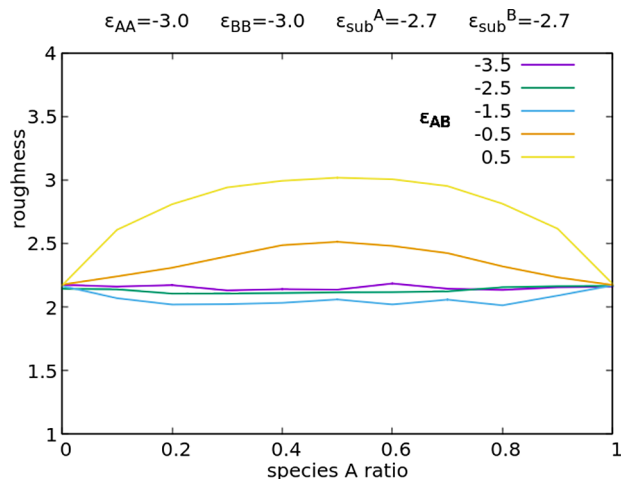


**Figure 4.** Roughness in monolayers (ML) as a function of concentration of the species A after deposition of 15 ML. Combination of two species with 3D growth, variation of  $\epsilon_{AB}$ . Other parameters:  $\Gamma = 10^3$ ,  $E^{ES} = 3.0$ , system size  $300^2$ ,  $E_{ij}^{ES} = E^{ES}$ .

combine two species which show 3D growth (similar to PEN and DIP) and vary the interspecies energy from mixing conditions ( $\epsilon_{AB} = -3.5$ ) to strong demixing ( $\epsilon_{AB} = 0.5$ ). Only in the demixing case, there is a noticeable increase of the roughness (this is important for rod–sphere mixtures); otherwise, it is insensitive. A simulation example for the combination of a material with 3D with an LBL growing material is shown in Figure S4.

To test the effect of the diffusion rate, we choose energetic parameters which correspond to a well–mixing system (Figure 5) and increase the ratio of diffusion constants  $D_B/D_A$ . The resulting roughness shows an approximately monotonic variation with concentration which, however, is not linear. Again, no decrease of roughness upon addition of a second species is found as in the experiment. Nevertheless,  $D_B \neq D_A$  implies that there could be different time scales for the development of 3D growth or the formation of islands. Thus, one can expect fine-tuning effects as exemplified in the parameter sets for the picene mixtures where the diffusion constant for picene was chosen such that it shows very strong island formation (Table S3).

We conclude that the roughness is insensitive to both diffusion rate and interaction strength (for mixing systems) in our growth regime and cannot explain the drastic roughness decrease we observe experimentally. Therefore, another mechanism must play a role, which is addressed below.

**Step Edge Barrier.** Finally another possible reason for the reduced roughness might be a modified step edge barrier. For pure materials, the step edge barrier is often significant and can lead to fast roughening.<sup>8,17–19,51</sup>

The variation of the interspecies step edge barrier ( $E_{ij}^{ES}$ ) in the simulations leads to the generic roughness effect seen in the experiment, i.e., the reduction of roughness upon mixing

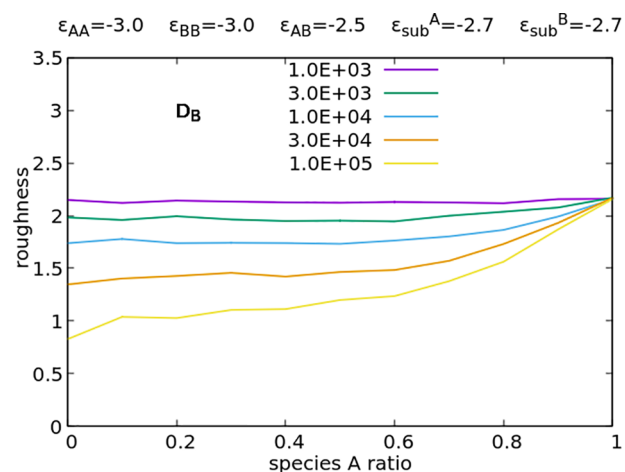


**Figure 5.** Roughness in ML as a function of concentration of the species A after deposition of 15 ML. Combination of one species with 3D growth with another which varies from 3D growth to LBL upon variation of  $D_B$ . The diffusion constant for the first species is set to  $D_A/F = 10^3$ , corresponding to 3D growth. The diffusion constant for the second species is varied between  $D_B/F = 10^3$  (3D growth) and  $10^5$  (LBL growth). Other parameters:  $E^{ES} = 3.0$ , system size  $300^2$ ,  $E_{ij}^{ES} = E^{ES}$ .

(Figure 6). We have seen that for energetic conditions suitable for mixing there is no strong variation of the roughness with

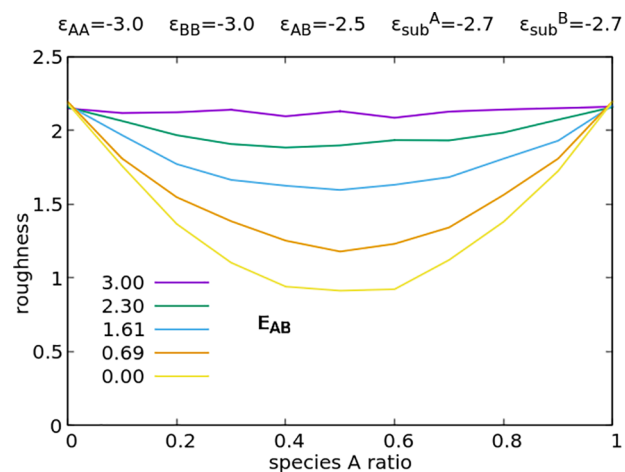


**Figure 6.** Roughness in ML as a function of concentration of the species A after deposition of 15 ML. Combination of two species with 3D growth. The ES barrier  $E_{AB}^{ES} = E_{BA}^{ES}$  is varied from 0.0 to 3.0, i.e., interlayer hops of one species on top of (or from) a particle from the other species are more likely. Other parameters:  $\Gamma = 10^3$ ,  $D = D_A = D_B$ ,  $E_{ii}^{ES} = 3.0$ , system size =  $300^2$ .

the interspecies energy. In this case, the condition  $E_{ij}^{ES} < E_{ii}^{ES}$  is the only possible cause of roughness reduction. We conclude that for a reduced and species dependent step edge barrier our KMC simulations are in excellent agreement with experimental data for the rod–rod mixed systems without co-crystallization (Figure 3a–d).

To rationalize the lowered step edge in the blends, we recall that the step edge barrier should be viewed as an effective quantity that arises through a weighted average over different step conformations.<sup>3</sup> In particular, molecular thin films have a distribution of different step edge barriers, dependent on the crystal orientation and the trajectory of the diffusing molecule

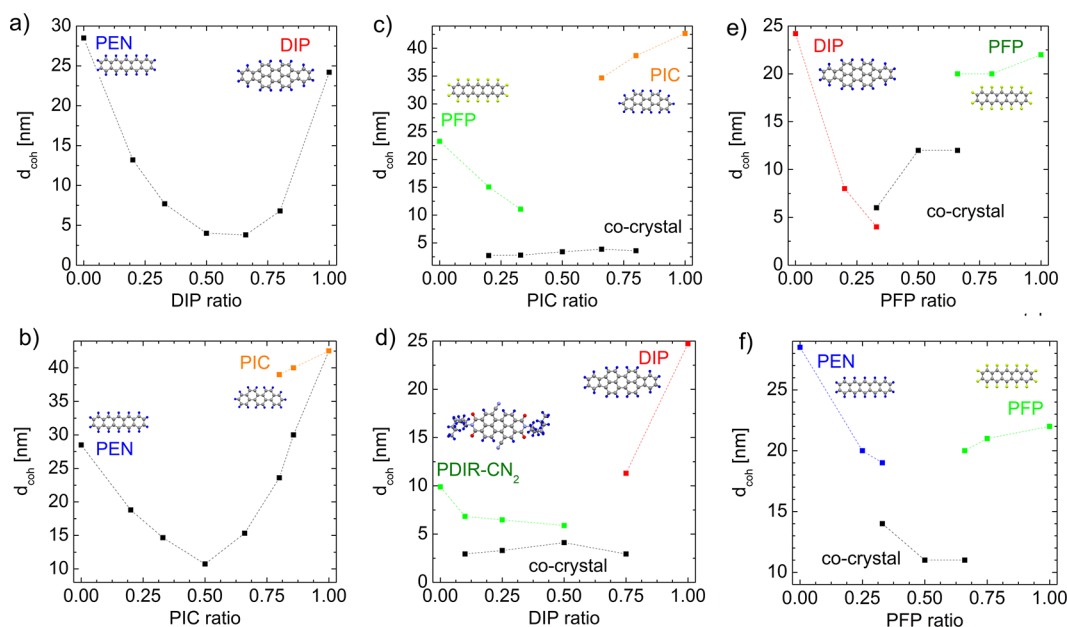


**Figure 7.** Coherent island size  $d_{\text{coh}}$  with rod-like compounds dependent on mixing ratio: (a) PEN:DIP,<sup>28</sup> (b) PEN:PIC,<sup>29,30</sup> (c) PFP:PIC,<sup>29</sup> (d) DIP:PDIR,<sup>31</sup> (e) DIP:PFP,<sup>32,33</sup> and (f) PEN:PFP.<sup>34</sup> From (a) to (f), the in-plane co-crystallization is increasing, i.e., PEN:DIP (a) is nearly randomly intermixing, whereas PEN:PFP (f) exhibits well ordered co-crystallization and (b)–(e) are intermediate cases. Black lines correspond to  $d_{\text{coh}}$  of the mixed domains or co-crystals. Colored lines correspond to  $d_{\text{coh}}$  of the respective molecularly pure domains.

over the step edge.<sup>8</sup> For a well-defined pure crystalline domain, the step edge barrier is relatively high. When we randomly introduce guest molecules into a molecular crystal (and also at the domain boundaries), the number of possible step conformations will increase, since guest molecules do not fit exactly into the lattice of the host and distort it. Therefore, it is natural to assume that with an increasing amount of guest molecules the distribution of step edge barriers broadens and some barriers are lower compared to the pure crystal. This effect should be strongest for large mixing ratios ( $\approx 1:1$ ). Since the diffusion lengths of organic molecules are relatively large,<sup>52</sup> the introduction of only a few low potential barriers, has a strong impact on the molecular downhill transport. Thus, the film roughening will be reduced.

It should be noted that this scenario is distinct from the well-known effect of surfactant molecules in metal homoepitaxy, which segregate at step edges and systematically modify the barrier for descending atoms.<sup>53</sup> Here, we do not expect the step edge barriers in the mixed films to be lower on average. Rather, the broadening of the distribution of barriers induced by the molecular disorder opens pathways for facile descent that are preferentially used by thermal activation. Since the solid-on-solid model does not account for the orientational degrees of freedom of the molecules, in our simulations this effect is nevertheless represented by an overall reduction of the barrier.

As a measure for the increased defect density we use the coherently scattering island size  $d_{\text{coh}}$  of the blends (Figure 7) which is derived from the fwhm of in-plane Bragg reflections. We observe that indeed  $d_{\text{coh}}$  decreases in the blends correlated to the decreasing roughness. For example, for statistically intermixing compounds such as PEN:DIP (Figure 3a), we find a minimum of  $d_{\text{coh}}$  near the 1:1 ratio (Figure 7a), which is consistent with the above explanation of the generation of smaller step edge barriers by guest molecules.

**Impact of Co-crystal Formation.** The observation of a local maximum in the roughness can again be discussed in terms of the in-plane crystallinity (Figure 7). For PEN:PFP and DIP:PFP, we find a strong tendency toward the formation of a 1:1 co-crystal with a relatively large  $d_{\text{coh}} > 10$  nm. Excess molecules of either compound phase separate in pure domains.<sup>32–34,54</sup> Due to this growth behavior, the crystallinity is increased at 1:1 ratio in these mixtures in comparison to statistically mixed compounds. Then, the effect of low potential step edge barriers introduced by guest molecules is weaker. The observation of increased roughness with higher crystallinity, supports the assumption that low step edge barriers are the main smoothing mechanism in organic mixed films of two rod-like molecules.

For the simulations, strong mixing conditions are characterized by  $\epsilon_{\text{AB}} \ll (\epsilon_{\text{AA}} + \epsilon_{\text{BB}})/2$ . In that limit, the lattice model shows a stable checkerboard phase which is similar to the 1:1 co-crystal formed in the PFP mixtures. There is one important difference. Experimental PFP mixtures not at equal (1:1) concentrations show phase separation into a pure component and the 1:1 co-crystal. The lattice model does not show a similar phase separation, rather, the checkerboard structure is randomly mixed in the system.

Since the co-crystallization is the most important difference of the PFP mixtures with PEN and DIP compared to the other mixing blends with PEN and/or DIP, we take the PEN:DIP parameters (including unequal ES barriers) but decrease  $\epsilon_{\text{AB}}$  substantially. The result is shown in Figure 8. Overall, there is no substantial change to the PEN:DIP curve, but, curiously, for the lowest  $\epsilon_{\text{AB}}$  a small hump is forming for  $c_{\text{A}} = 0.5$ . The effect seems to be genuine and persists also for a choice of less unequal ES barriers. Nevertheless, it is too small compared to the experimentally observed effect.

Therefore, the PFP:DIP and PFP:PEN mixtures should rather be considered as weakly phase separating mixtures of the pure compound with the respective 1:1 co-crystal, and the

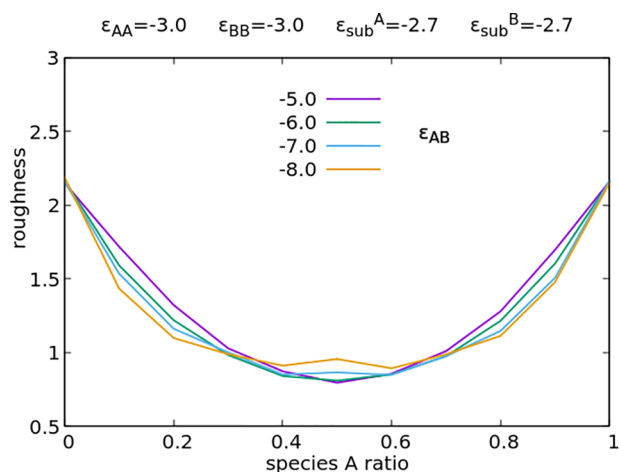


**Figure 8.** Roughness in ML as a function of concentration of the species A after deposition of 15 ML. Combination of two species with 3D growth, variation of  $\epsilon_{AB}$  in the strong mixing regime. Other parameters:  $\Gamma = 10^3$ ,  $E_{ii}^{ES} = 3.0$ ,  $E_{ij}^{ES} = 0.0$  ( $i \neq j$ ), system size =  $300^2$ .

roughness behavior of these mixtures is more similar to those of weakly phase separating mixtures like DIP:C<sub>60</sub> described below.

**Sphere-like with Rod-like Compound: Phase Separation.** Qualitatively different from intermixing rod/rod blends discussed above are rod/sphere such as mixtures realized with C<sub>60</sub> and a rod-shaped compound. Due to geometrical constraints, rod/sphere blends are typically phase separating in thermal equilibrium but, due to kinetic effects, are partially intermixed in thin films.<sup>55</sup> Figure 3g–i shows the roughness of mixed films of C<sub>60</sub> with three different rod-shaped compounds (DIP, 6T, PEN). We observe that for a small amount of guest molecules the roughness is decreased, which can be explained consistently by a reduced in-plane crystallinity.

For a phase separating system, the roughness depends on the domain size and therefore the degree of phase separation, which is related to the interspecies interaction energy.<sup>56</sup> From KMC simulations, we conclude that the smoothing effect induced by a low step edge barrier (Figure 6) and the roughening effect induced by unfavorable interspecies energies

(Figures 4 and S4), i.e., phase separation, are competing effects. Both effects can be active to a different degree dependent on mixing ratio.

The three mixtures studied (Figure 3g–i) exhibit nanophase separation into pure domains dependent on the growth conditions.<sup>55,57–59</sup> For DIP:C<sub>60</sub>, 6T:C<sub>60</sub> and mixing ratios deviating from 1:1, we observe smaller roughness values compared to the pure compounds, induced due to larger disorder and therefore smaller step edges as described above. For DIP:C<sub>60</sub>, the driving force for phase separation (dependent on the interspecies energy) is weak, resulting in small  $d_{\text{coh}}$  (Figure S2). In contrast, for PEN:C<sub>60</sub>, the interspecies energies are apparently strongly unfavorable for mixing, leading to a large  $d_{\text{coh}}$  and the largest roughness of the three systems studied. We note that this strong phase separation in PEN:C<sub>60</sub> is observed even though a chemical reaction between PEN and C<sub>60</sub> molecules might be present at domain boundaries.<sup>60</sup>

These observations are also consistent with KMC simulations with a variation of the ES barrier (Figure 6). For energetic conditions suitable for demixing, we have seen that the roughness of blended films is higher and the degree of roughness increase depends on the propensity for phase separation (i.e., the value of  $\epsilon_{AB} - (\epsilon_{AA} + \epsilon_{BB})/2$ ) but also on the single species growth mode. Therefore, we have here two competing mechanisms influencing the final roughness. For weakly phase separating systems, the ES effect could dominate, but for strongly phase separating systems it can be the other way around. This is also seen in the experiments.

For 1:1 mixing ratios, we find a local roughness maximum for all three mixed systems. For DIP:C<sub>60</sub>, it was shown that at 1:1 mixing ratios the films exhibit two types of domains: a nanophase separated wetting layer and pure domains of DIP.<sup>61</sup> Similarly, in AFM data of PEN:C<sub>60</sub> (Figure 9), we also observe a pronounced 3D growth of pure PEN domains near the 1:1 mixing ratio in combination with a mixed wetting layer.<sup>57</sup>

Based on our simulations, we assume that phase separated PEN domains in the first monolayers are further templating the growth of pure PEN domains in the vertical direction. Therefore, we assume the buried region under large PEN domains likely consists of pure PEN domains.

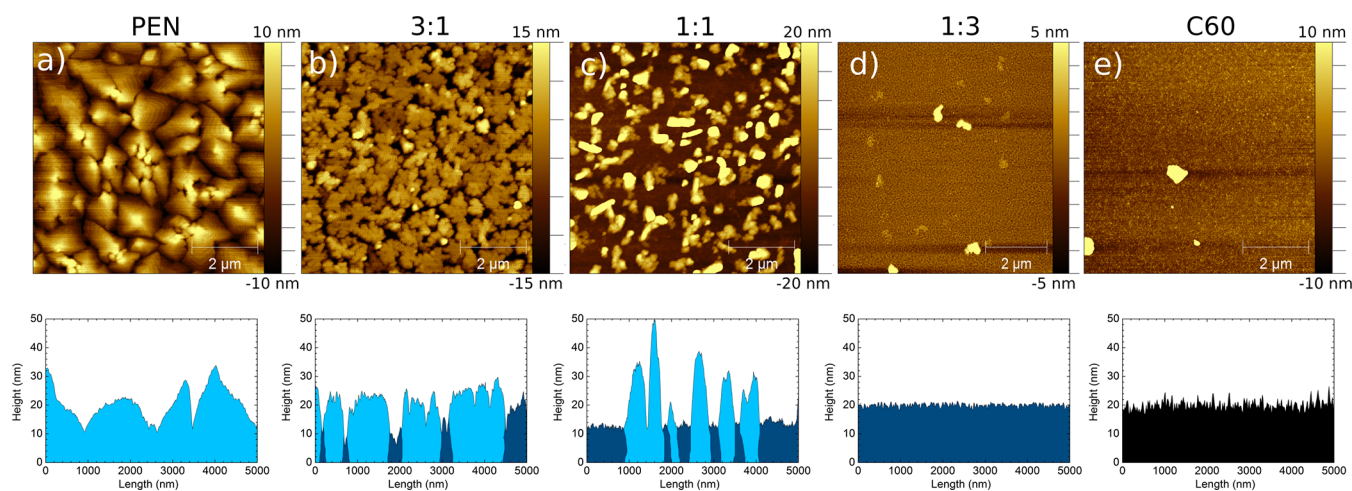


**Figure 9.** AFM images of (a) PEN, (e) C<sub>60</sub>, and three PEN:C<sub>60</sub> mixtures (b–d) with different mixing ratios. Sketches below each AFM image show typical line scans. Colors indicate the assumed domain compositions: light blue (pure PEN), dark blue (nanophase separated mixture), and black (C<sub>60</sub>).

The strong 3D growth of the pure domains in these films is the main cause for the local roughness increase. Since the lateral separation between these domains is on the order of  $\approx 1000$  lattice sites, this effect cannot be completely captured by our KMC simulations. However, we find that the increase in roughness at the 1:1 ratio scales overall with the driving force for phase separation (weak for DIP:C60, strong for PEN:C60) and depends presumably mainly on the interspecies interaction energies. We conclude that the roughening and smoothing mechanisms are qualitatively the same for all three mixtures studied but quantitatively of course dependent on material properties.

## CONCLUSIONS

We presented an extensive and systematic study on the roughness evolution of different organic mixed thin films. We distinguished the roughening mechanism in intermixing rod/rod blends and phase separating rod/sphere blends. KMC simulations revealed that a species dependent step edge barrier is the main smoothing mechanism. As a possible scenario, we propose a broadening of the distribution of step edge barriers induced by guest molecules. This idea is supported by the strong correlation between in-plane coherent crystal length and roughness for all studied blends. For intermixing rod/rod blends, we find a roughness minimum close to the 1:1 ratio induced by a reduced step edge barrier. For rod/sphere blends, the roughness depends, in addition to the reduced step edge barrier, on the competing effect of phase separation. Finally, a local roughness maximum at the 1:1 ratio was found also for co-crystallizing blends. These blends behave similar to weakly phase separating blends, where phase separation occurs between a 1:1 co-crystal and the pure compound (see also Figure 3).

Our study shows an intriguing and subtle connection between nonequilibrium structure formation and equilibrium phase behavior mediated by the kinetics of interlayer transport. Importantly, the near-universal smoothing observed in the mixed films relies on the thermally activated character of step crossing events, which implies that the transport is effectively dominated by the lowest available barriers. In this regard, systematic growth experiments at different temperatures could lead to insights on the distribution of the step edge barriers. We expect that similar scenarios observed here may be found in other systems where complex molecular interactions give rise to a broad distribution of kinetic rates.

## ASSOCIATED CONTENT

### Supporting Information

The Supporting Information is available free of charge at <https://pubs.acs.org/doi/10.1021/acs.jpcc.2c02177>.

Additional data on growth rates, in-plane coherent island sizes, and in-plane correlation length of the samples; simulation parameters and results of additional MC simulations (PDF)

## AUTHOR INFORMATION

### Corresponding Author

Alexander Hinderhofer – Institute for Applied Physics, University of Tübingen, 72076 Tübingen, Germany; [orcid.org/0000-0001-8152-6386](https://orcid.org/0000-0001-8152-6386); Email: [alexander.hinderhofer@uni-tuebingen.de](mailto:alexander.hinderhofer@uni-tuebingen.de)

## Authors

Jan Hagenlocher – Institute for Applied Physics, University of Tübingen, 72076 Tübingen, Germany

Alexander Gerlach – Institute for Applied Physics, University of Tübingen, 72076 Tübingen, Germany; [orcid.org/0000-0003-1787-1868](https://orcid.org/0000-0003-1787-1868)

Joachim Krug – Institute for Biological Physics, University of Cologne, 50937 Köln, Germany

Martin Oettel – Institute for Applied Physics, University of Tübingen, 72076 Tübingen, Germany

Frank Schreiber – Institute for Applied Physics, University of Tübingen, 72076 Tübingen, Germany; [orcid.org/0000-0003-3659-6718](https://orcid.org/0000-0003-3659-6718)

Complete contact information is available at:

<https://pubs.acs.org/doi/10.1021/acs.jpcc.2c02177>

## Notes

The authors declare no competing financial interest.

## ACKNOWLEDGMENTS

Support from the DFG (HI 1927/1-1) and the BMBF is gratefully acknowledged. We thank M. Kotrla for fruitful discussions and numerous members of the Tübingen group for contributing data. We are grateful for beamtimes granted by the ESRF (Grenoble, France) and Swiss Light Source (Villigen, Switzerland) and helpful assistance of the staff of the ID10 (Oleg Kononov, ESRF) and MS X04SA (Phil Willmott, SLS) beamlines.

## REFERENCES

- (1) Barabasi, A.-L.; Stanley, H. E. *Fractal concepts in surface growth*; Cambridge University Press: Cambridge, 1995.
- (2) Pimpinelli, A.; Villain, J. *Physics of Crystal Growth*; Cambridge University Press, Cambridge, 1998.
- (3) Michely, T.; Krug, J. *Islands, Mounds, and Atoms. Patterns and Processes in Crystal Growth Far from Equilibrium*; Springer: Berlin, 2004.
- (4) Krug, J. Origins of scale invariance in growth processes. *Adv. Phys.* **1997**, *46*, 139–282.
- (5) Zhao, Y.; Wang, G.-C.; Lu, T.-M. *Characterization of Amorphous and Crystalline Rough Surface: Principles and Applications*; Academic Press: San Diego, 2001.
- (6) Pimpinelli, A.; Tumbek, L.; Winkler, A. Scaling and Exponent Equalities in Island Nucleation: Novel Results and Application to Organic Films. *J. Phys. Chem. Lett.* **2014**, *5*, 995–998.
- (7) Hlawacek, G.; Puschnig, P.; Frank, P.; Winkler, A.; Ambrosch-Draxl, C.; Teichert, C. Characterization of Step-Edge Barriers in Organic Thin-Film Growth. *Science* **2008**, *321*, 108–111.
- (8) Hlawacek, G.; Teichert, C. Nucleation and growth of thin films of rod-like conjugated molecules. *J. Phys. Condens. Matter* **2013**, *25*, 143202.
- (9) Hinderhofer, A.; Gerlach, A.; Kowarik, S.; Zontone, F.; Krug, J.; Schreiber, F. Smoothing and coherent structure formation in organic-organic heterostructure growth. *Europhys. Lett.* **2010**, *91*, 56002.
- (10) Yim, S.; Jones, T. S. Growth dynamics of C<sub>60</sub> thin films: Effect of molecular structure. *Appl. Phys. Lett.* **2009**, *94*, 021911.
- (11) Yang, J.; Yim, S.; Jones, T. S. Molecular-Orientation-Induced Rapid Roughening and Morphology Transition in Organic Semiconductor Thin-Film Growth. *Sci. Rep.* **2015**, *5*, 9441.
- (12) Zhang, Y.; Barrena, E.; Zhang, X.; Turak, A.; Maye, F.; Dosch, H. New Insight into the Role of the Interfacial Molecular Structure on Growth and Scaling in Organic Heterostructures. *J. Phys. Chem. C* **2010**, *114*, 13752–13758.
- (13) Nahm, R. K.; Bullen, H. J.; Suh, T.; Engstrom, J. R. Faster Is Smoother and So Is Lower Temperature: The Curious Case of Thin

Film Growth of Tetracene on SiO<sub>2</sub>. *J. Phys. Chem. C* **2017**, *121*, 8464–8472.

(14) Hinderhofer, A.; Hosokai, T.; Yonezawa, K.; Gerlach, A.; Kato, K.; Broch, K.; Frank, C.; Novák, J.; Kera, S.; Ueno, N.; et al. Post-growth surface smoothing of thin films of diindenoperylene. *Appl. Phys. Lett.* **2012**, *101*, 033307.

(15) Dürr, A. C.; Schreiber, F.; Ritley, K. A.; Kruppa, V.; Krug, J.; Dosch, H.; Struth, B. Rapid Roughening in Thin Film Growth of an Organic Semiconductor (Diindenoperylene). *Phys. Rev. Lett.* **2003**, *90*, 016104.

(16) Storzer, T.; Hinderhofer, A.; Zeiser, C.; Novák, J.; Fišer, Z.; Belova, V.; Reisz, B.; Maiti, S.; Duva, G.; Hallani, R. K.; et al. Growth, Structure, and Anisotropic Optical Properties of Difluoro-anthradi-thiophene Thin Films. *J. Phys. Chem. C* **2017**, *121*, 21011–21017.

(17) Fendrich, M.; Krug, J. Ehrlich-Schwoebel effect for organic molecules: Direct calculation of the step-edge barrier using empirical potentials. *Phys. Rev. B* **2007**, *76*, 121302.

(18) Roscioni, O. M.; D'Avino, G.; Muccioli, L.; Zannoni, C. Pentacene Crystal Growth on Silica and Layer-Dependent Step-Edge Barrier from Atomistic Simulations. *J. Phys. Chem. Lett.* **2018**, *9*, 6900–6906.

(19) Goose, J. E.; First, E. L.; Clancy, P. Nature of step-edge barriers for small organic molecules. *Phys. Rev. B* **2010**, *81*, 205310.

(20) Ehrlich, G.; Hudda, F. G. Atomic View of Surface Self-Diffusion: Tungsten on Tungsten. *J. Chem. Phys.* **1966**, *44*, 1039–1049.

(21) Schwoebel, R. L.; Shipsey, E. J. Step Motion on Crystal Surfaces. *J. Appl. Phys.* **1966**, *37*, 3682–3686.

(22) Winkler, A. On the nucleation and initial film growth of rod-like organic molecules. *Surf. Sci.* **2016**, *652*, 367–377.

(23) Conrad, B. R.; Gomar-Nadal, E.; Cullen, W. G.; Pimpinelli, A.; Einstein, T. L.; Williams, E. D. Effect of impurities on pentacene island nucleation. *Phys. Rev. B* **2008**, *77*, 205328.

(24) Kleemann, H.; Schuenemann, C.; Zakhidov, A. A.; Riede, M.; Lüssem, B.; Leo, K. Structural phase transition in pentacene caused by molecular doping and its effect on charge carrier mobility. *Org. Electron.* **2012**, *13*, 58–65.

(25) Schwarze, M.; Tress, W.; Beyer, B.; Gao, F.; Scholz, R.; Poelking, C.; Ortstein, K.; Gunther, A. A.; Kasemann, D.; Andrienko, D.; et al. Band structure engineering in organic semiconductors. *Science* **2016**, *352*, 1446–1449.

(26) Zhang, J.; Xu, W.; Sheng, P.; Zhao, G.; Zhu, D. Organic Donor-Acceptor Complexes as Novel Organic Semiconductors. *Acc. Chem. Res.* **2017**, *50*, 1654–1662.

(27) Hinderhofer, A.; Schreiber, F. Organic-organic heterostructures: Concepts and applications. *ChemPhysChem* **2012**, *13*, 628–643.

(28) Aufderheide, A.; Broch, K.; Novák, J.; Hinderhofer, A.; Nervo, R.; Gerlach, A.; Banerjee, R.; Schreiber, F. Mixing-Induced Anisotropic Correlations in Molecular Crystalline Systems. *Phys. Rev. Lett.* **2012**, *109*, 156102.

(29) Dieterle, J.; Broch, K.; Hinderhofer, A.; Frank, H.; Novák, J.; Gerlach, A.; Breuer, T.; Banerjee, R.; Witte, G.; Schreiber, F. Structural Properties of Picene-Perfluoropentacene and Picene-Pentacene Blends: Superlattice Formation versus Limited Interdiffusion. *J. Phys. Chem. C* **2015**, *119*, 26339–26347.

(30) Dieterle, J.; Broch, K.; Frank, H.; Duva, G.; Storzer, T.; Hinderhofer, A.; Novák, J.; Gerlach, A.; Schreiber, F. Delayed phase separation in growth of organic semiconductor blends with limited interdiffusion. *Phys. Status Solidi RRL* **2017**, *11*, 1600428.

(31) Belova, V.; Beyer, P.; Meister, E.; Linderl, T.; Halbich, M.-U.; Gerhard, M.; Schmidt, S.; Zechel, T.; Meisel, T.; Generalov, A. V.; et al. Evidence for Anisotropic Electronic Coupling of Charge Transfer States in Weakly Interacting Organic Semiconductor Mixtures. *J. Am. Chem. Soc.* **2017**, *139*, 8474–8486.

(32) Reinhardt, J. P.; Hinderhofer, A.; Broch, K.; Heinemeyer, U.; Kowarik, S.; Vorobiev, A.; Gerlach, A.; Schreiber, F. Structural and Optical Properties of Mixed Diindenoperylene-Perfluoropentacene Thin Films. *J. Phys. Chem. C* **2012**, *116*, 10917–10923.

(33) Broch, K.; Gerlach, A.; Lorch, C.; Dieterle, J.; Novák, J.; Hinderhofer, A.; Schreiber, F. Structure formation in perfluoropentacene:diindenoperylene blends and its impact on transient effects in the optical properties studied in real-time during growth. *J. Chem. Phys.* **2013**, *139*, 174709.

(34) Hinderhofer, A.; Frank, C.; Hosokai, T.; Resta, A.; Gerlach, A.; Schreiber, F. Structure and morphology of coevaporated pentacene-perfluoropentacene thin films. *J. Chem. Phys.* **2011**, *134*, 104702.

(35) Kitaigorodsky, A. In *Mixed Crystals*; Cordona, M., Ed.; Springer: Berlin, Heidelberg, 1984.

(36) Janke, W.; Speck, T. Multiscale modeling of structure formation of C60 on insulating CaF<sub>2</sub> substrates. *J. Chem. Phys.* **2021**, *154*, 234701.

(37) Viani, L.; Risko, C.; Toney, M. F.; Breiby, D. W.; Bredas, J.-L. Substrate-Induced Variations of Molecular Packing, Dynamics, and Intermolecular Electronic Couplings in Pentacene Monolayers on the Amorphous Silica Dielectric. *ACS Nano* **2014**, *8*, 690–700.

(38) Ikeda, S. Molecular dynamics simulations of pentacene thin film growth: Stability of nuclei comprising standing molecules and their subsequent growth. *Appl. Phys. Express* **2020**, *13*, 015508.

(39) Ritley, K. A.; Krause, B.; Schreiber, F.; Dosch, H. A portable ultrahigh vacuum organic molecular beam deposition system for *in situ* x-ray diffraction measurements. *Rev. Sci. Instrum.* **2001**, *72*, 1453–1457.

(40) Nelson, A. Co-refinement of multiple-contrast neutron/X-ray reflectivity data using MOTOFIT. *J. Appl. Crystallogr.* **2006**, *39*, 273–276.

(41) Nečas, D.; Klapetek, P. Gwyddion: an open-source software for SPM data analysis. *Cent. Eur. J. Phys.* **2012**, *10*, 181–188.

(42) Smilgies, D.-M. Scherrer grain-size analysis adapted to grazing-incidence scattering with area detectors. *J. Appl. Crystallogr.* **2009**, *42*, 1030–1034.

(43) Empting, E.; Klopotek, M.; Hinderhofer, A.; Schreiber, F.; Oettel, M. Lattice gas study of thin-film growth scenarios and transitions between them: Role of substrate. *Phys. Rev. E* **2021**, *103*, 023302.

(44) Assis, T. A. d.; Aarão Reis, F. D. A. Dynamic scaling and temperature effects in thin film roughening. *J. Stat. Mech.* **2015**, *2015*, P06023.

(45) Hosokai, T.; Hinderhofer, A.; Vorobiev, A.; Lorch, C.; Watanabe, T.; Koganezawa, T.; Gerlach, A.; Yoshimoto, N.; Kubozono, Y.; Schreiber, F. In situ structural characterization of picene thin films by X-ray scattering: Vacuum versus O<sub>2</sub> atmosphere. *Chem. Phys. Lett.* **2012**, *544*, 34–38.

(46) Kurihara, R.; Hosokai, T.; Kubozono, Y. Growth and Structure of Picene Thin Films on SiO<sub>2</sub>. *Mol. Cryst. Liq. Cryst.* **2013**, *580*, 83–87.

(47) Hosokai, T.; Hinderhofer, A.; Bussolotti, F.; Yonezawa, K.; Lorch, C.; Vorobiev, A.; Hasegawa, Y.; Yamada, Y.; Kubozono, Y.; Gerlach, A.; et al. Thickness and Substrate Dependent Thin Film Growth of Picene and Impact on the Electronic Structure. *J. Phys. Chem. C* **2015**, *119*, 29027–29037.

(48) Kotrla, M.; Krug, J.; Smilauer, P. Effects of mobile and immobile impurities on two-dimensional nucleation. *Surf. Sci.* **2001**, *482–485*, 840–843.

(49) Käfer, D.; Ruppel, L.; Witte, G. Growth of pentacene on clean and modified gold surfaces. *Phys. Rev. B* **2007**, *75*, 085309.

(50) Watanabe, T.; Kikuchi, M.; Nishida, K.; Koganezawa, T.; Hirozawa, I.; Yoshimoto, N. A new instrumentation for characterization of the charge transport and crystallographic properties in co-evaporated organic thin film transistor. *Mol. Cryst. Liq. Cryst.* **2016**, *636*, 168–175.

(51) Yim, S.; Kim, K.; Jones, T. S. Growth Morphology of Perylene-3,4,9,10-tetracarboxylic Dianhydride (PTCDA) Thin Films: Influence of Intermolecular Interactions and Step-Edge Barriers. *J. Phys. Chem. C* **2007**, *111*, 10993–10997.

(52) Meyer zu Heringdorf, F.-J.; Reuter, M. C.; Tromp, R. M. Growth dynamics of pentacene thin films. *Nature* **2001**, *412*, 517–520.

(53) Esch, S.; Hohage, M.; Michely, T.; Comsa, G. Origin of oxygen induced layer-by-layer growth in homoepitaxy on Pt(111). *Phys. Rev. Lett.* **1994**, *72*, 518–521.

(54) Breuer, T.; Witte, G. Thermally activated intermixture in pentacene-perfluoropentacene heterostructures. *J. Chem. Phys.* **2013**, *138*, 114901.

(55) Banerjee, R.; Novák, J.; Frank, C.; Lorch, C.; Hinderhofer, A.; Gerlach, A.; Schreiber, F. Evidence for Kinetically Limited Thickness Dependent Phase Separation in Organic Thin Film Blends. *Phys. Rev. Lett.* **2013**, *110*, 185506.

(56) Kotrla, M.; Slanina, F.; Predota, M. Scaling in a two-component surface-growth model. *Phys. Rev. B* **1998**, *58*, 10003–10011.

(57) Salzmann, I.; Duhm, S.; Opitz, R.; Johnson, R. L.; Rabe, J. P.; Koch, N. Structural and electronic properties of pentacene-fullerene heterojunctions. *J. Appl. Phys.* **2008**, *104*, 114518.

(58) Lorch, C.; Frank, H.; Banerjee, R.; Hinderhofer, A.; Gerlach, A.; Li Destri, G.; Schreiber, F. Controlling length-scales of the phase separation to optimize organic semiconductor blends. *Appl. Phys. Lett.* **2015**, *107*, 201903.

(59) Lorch, C.; Broch, K.; Belova, V.; Duva, G.; Hinderhofer, A.; Gerlach, A.; Jankowski, M.; Schreiber, F. Growth and annealing kinetics of  $\alpha$ -sexithiophene and fullerene C mixed films. *J. Appl. Phys.* **2016**, *49*, 1266–1275.

(60) Breuer, T.; Geiger, T.; Bettinger, H.; Witte, G. Diels–Alder adduct formation at solid interfaces between fullerenes and acenes. *J. Condens. Matter Phys.* **2019**, *31*, 034003.

(61) Banerjee, R.; Hinderhofer, A.; Weinmann, M.; Reisz, B.; Lorch, C.; Gerlach, A.; Oettel, M.; Schreiber, F. Interrupted Growth to Manipulate Phase Separation in DIP:C60 Organic Semiconductor Blends. *J. Phys. Chem. C* **2018**, *122*, 1839–1845.